Catalysis Science & Technology

Accepted Manuscript

ROYAL SOCIETY OF CHEMISTRY

www.rsc.org/catalysis

Cite this: DOI: 10.1039/c0xx00000x

www.rsc.org/xxxxxx

ARTICLE TYPE

Metal-free carbon nanotubes/SiC nanowires composite photocatalyst with enhanced photocatalytic H_2 evolution under visible light irradiation

Xunfu Zhou, Xin Li,* Qiongzhi Gao, Jielin Yuan, Jiuqing Wen, Yueping Fang,* Wei Liu, Shengsen Zhang, Yingju Liu

Received (in XXX, XXX) Xth XXXXXXXXX 20XX, Accepted Xth XXXXXXXXX 20XX
DOI: 10.1039/b000000x

In this report, metal-free multi-walled carbon nanotubes (MWCNTs)/ SiC nanowires 1D-1D nanoheterostructures were successfully synthesized by an *in situ* chemical reaction between MWCNTs and silicon powders. The vapor-liquid-solid (VLS) mechanism was found to be responsible for the *in situ* growth of the SiC nanowires along MWCNTs. The structure, morphology and composition of the as-obtained MWCNTs/SiC 1D-1D samples were characterized by X-ray powder diffraction (XRD), transmission electron microscopy (TEM), thermal gravimetric analysis (TGA) and UV-Vis absorption spectra. The photoactivities of the resultant MWCNTs/SiC nanoheterostructures for H_2 evolution under the visible light irradiation were also investigated. Results showed that the metal-free MWCNTs/SiC 1D-\1D nanoheterostructures exhibited the highest H_2-evolution rate among all samples, up to108 μmol/g.h, which was 3.1 times higher than that of pure SiC without MWCNTs. It suggests that the activity enhancement of the MWCNTs/SiC 1D-1D nanocomposites for hydrogen evolution under visible light irradiation is mainly attributed to the synergistic effects of enhanced separation efficiency of photogenerated hole-electron pairs at the MWCNTs/SiC interfaces, improved crystallinity, unique 1D-1D nanoheterostructures and increased visible light absorption. The present work not only gives new insights into the underlying photocatalysis mechanism of metal-free MWCNTs/SiC 1D-1D nanoheterostructures, but also provides a versatile strategy to design 1D-1D nanocomposite photocatalysts, with great potential applications in photocatalytic H_2 generation or degradation of environmental pollutants.

1. Introduction

The shortage of the energy supply and the disastrous environmental pollution have been regarded as two main challenges in the near further. From a sustainability viewpoint, both problems could be simultaneously addressed by the heterogeneous photocatalysis technique.[1-3] In particular, as a typical artificial photosynthesis system, photocatalytic hydrogen generation from water splitting has received increasing research attention since Honda and Fujishima pioneerly discovered photoelectrocatalytic H_2 evolution over TiO_2 in 1972.[4] One of the biggest bottlenecks in heterogeneous photocatalysis systems for water splitting lies in their low quantum yields, due to the weak absorption in visible region, the fast surface and bulk recombination of photo-generated electron−hole pairs and the undesirable surface back reactions.[1, 2] Thus far, a large number of research efforts have recently focused on developing visible-light-driven photocatalysts, enhancing the separation efficiency of photo-induced electron–hole pairs and accelerating surface reaction kinetics.[2, 5] Among all the semiconductor materials studied, TiO_2 is the most widely used photocatalyst and has been deeply investigated by different groups due to its excellent stability, innocuity and low price. However, its low quantum efficiency and wide band gap (3.0-3.2 eV) have significantly negative impacts on the effective utilization of solar energy. Therefore, to develop more efficient photocatalyst systems for hydrogen evolution through fully utilizing the abundant solar energy, extensive studies have been initiated on extending the absorption of TiO_2 into the visible region[6, 7] or finding new visible-light photocatalysts consisting of earth-abundant, less-expensive elements, such as g-C_3N_4,[8, 9] SiC,[10, 11] metal sulphide[12-14] and (oxy)nitride[5, 15, 16].

As a well-known n-type semiconductor, metal-free silicon carbide (SiC) has also attracted considerable interest in solar water splitting due to its adequate band gap (2.3 eV for 3C-SiC and 3.3 eV for 2H-SiC at room temperature),[17] relatively negative conduction band potential, high electron mobility, high chemical stability, and facile preparation by scalable methods. Furthermore, the low cost and excellent biocompatibility of SiC make it a potential material for large-scale applications in photocatlytic H_2 evolution. More importantly, the quantum confinement effect has been experimentally achieved in colloidal 3C-SiC nanocrystals with a size well below 10 nm.[18, 19] However, compared to TiO_2, there are only limited reports about the application of powdery SiC in photocatalysis due to its photocorrosion and fast recombination rate of photo-generated hole/electron pairs.[20, 21] Therefore, various different engineering strategies such as sensitization,[11] construction of

heterostructures,[11, 21-23] formation of unique nanostructures,[24-28] hybridization of co-catalysts[29, 30] and/or nanocarbon materials[10, 31] have been developed to enhance the photocatalytic activity and efficiency of SiC in water spliiting since the first application of β-SiC for water splitting under UV in 1990.[32] For instance, Gao et al. demonstrated that the photocatalytic H_2 production from splitting of pure water can be achieved over commercial green SiC micropowder (containing mainly 6H-SiC and some 3C-SiC) under visible light irradiation. They also observed a remarkable increase in the activity by the addition of OH^- or S^{2-} due to the effective oxidation of S^{2-} and adsorption of H^+ ions.[33] Guo and coworkers reported that the specific surface areas, morphologies and surface hydrophilic ability of SiC have significant influences on its photocatalytic H_2 evolution performance from pure water under visible light irradiation.[24, 26] The further results showed that the SiC-graphene nanocomposites exhibited enhanced activities for overall water splitting under visible light irradiation due to improved separation of photogenerated hole-electron pairs by the formation of Schottky-junction interface.[10, 31] Moreover, yuan et al revealed that the coupling of SiC with CdS can intensively enhance its photocatalytic H_2-evolution activity in the presence of a sacrificial reagent (Na_2S and Na_2SO_3) under visible light irradiation due to the increased active sites and accelerated separation of electron–hole pairs based on the direct Z-scheme mechanism.[11] Recently, we synthesized novel SnO_2/SiC hollow sphere nanochains by topological conversion of SnO_2@C core-shell nanochains through a vapour-solid reaction, which exhibited enhanced photocatalytic activity and durability for H_2 generation from a Na_2S solution due to improved spatial separation of photo-induced charge carriers.[23]

Meanwhile, it is well known that the hybridization of CNTs with various semiconductors has become a popular strategy to develop highly efficient carbon-based composite photocatalysts during the past few years.[34-36] This is because CNTs as a good support, an ideal building block or an electron-transfer channel possess many unique properties such as a large electron-storage capacity, good electron conductivity, good chemical stability, excellent mechanical strength, a large specific surface area (>150 m^2/g), and mesoporous character, which favors the adsorption/diffusion of reacting species and the effective separation of photo-generated hole-electron pairs, thus leading to an enhanced photoactivity.[37] More interestingly, CNTs can also be used as a carbon source for making different kinds of one-dimensional (1D) nanomaterials such as SiC. In 1995, Dai et al. firstly synthesized β-SiC nanorods with diameters from 2 to 20 nm and lengths of the order of 1 μm using a carbon nanotube confined reaction with SiO or Si +I_2 at 1100-1450 °C in a vacuum.[38] Meanwhile, one-dimensional SiC nanotubes and nanowires were also synthesized via the reaction of silicon with MWCNTs in the carrier gas of argon mixed with 5% H_2 at 1250 °C and 500 Torr.[39] The C-SiC coaxial nanotubes were also synthesized by the reaction of CNTs with un-contacted Si powders at 1200 °C in a vacuum.[40] However, to the best of our knowledge, there are few studies reporting the facile synthesis of SiC-CNTs nanocomposites in an Ar atmosphere at constant pressure and their specific application in the photocatalytic water splitting, although SiC-CNTs nanocomposites have been successfully prepared in a vacuum for almost twenty years.

In addition, the construction of 1D nanostrcutures or 1D-1D nanoheterostructures has received attention as a promising approach for the development of highly efficient photocatalysts because 1D structural photocatalysts exhibit many excellent properties such as a fast and long-distance electron transport, enhanced light absorption and scattering.[1, 41-44] Therefore, it is of utmost interest to synthesize metal-free SiC-CNTs 1D-1D nanocomposite photocatalysts by a simple chemical reaction between MWCNTs and silicon powders and further apply them in photocatalytic H_2 production under visible light irradiation. In the present study, we report a simple and scalable route to synthesize SiC-CNTs 1D-1D nanocomposites via an *in situ* chemical reaction between MWCNTs and silicon powders. The resultant SiC/CNTs 1D-1D nanocomposites were characterized by different techniques including transmission electron microscopy (TEM), X-ray diffraction (XRD) and UV–Vis absorption spectra. The photocatalytic activity of the as-prepared metal-free SiC/CNTs 1D-1D nanocomposites for water splitting under the visible light irradiation was also investigated. The results show that the SiC/CNTs nanocomposites exhibited significantly enhanced activities for photocatalytic hydrogen evolution from pure water. The photocatalysis enhancement mechanism of MWCNTs/SiC 1D-1D nanoheterostructures for water splitting was discussed in detail.

2. Experimental

2.1. Catalysts preparation

All chemicals are of analytical grade and used as received without further purification. Multi-walled carbon nanotubes (MWCNTs; purity, >95%; diameter, 40–60 nm; length, 5–15μm; specific surface area, 40–300 m^2/g) prepared by catalytic decomposition of CH_4 using La_2NiO_4 as catalyst precursor, were provided by Shenzhen Nanoport Co. Ltd. (NPT).

In a typical process, 0.4 g MWCNTs was mixed with superfluous silicon powder. Subsequently, the mixture was placed into the hot zone inside a ceramic tube of a horizontal furnace. Ar gas was introduced at one end of the tubular furnace flowing at 250 sccm (standard cubic centimeters per minute) and at a constant pressure of 0.1 MPa during the overall experiment. The temperature of furnace was increased to 1320 °C at 3°C/min rate and kept at this temperature for 360 min. After the reaction was terminated, the sample was cooled to room temperature in Ar. Finally, the as-obtained samples were washed with a mixed HF/HNO_3 solution, and dried at 120 °C for 12 h, and then were denoted as SiC-CNTs.

The pure SiC can be obtained after annealing the SiC-CNTs composites at 650 °C in air for 4h, which can remove the multi-walled CNTs from the composites by the oxidation of CNTs in air.

For preparation of referenced R-SiC, CNTs was firstly refluxed at 70 °C for 24 h, in the presence of concentrated HNO_3. Then, the as-obtained samples were treated with a mixed concentrated H_2SO_4/HNO_3 solution (3:1) at 70 °C for 1 h under ultrasonic radiation. Finally, the dry sample was denoted as acid-treated CNTs. The referenced R-SiC was obtained under the same conditions as SiC-CNTs using the acid-treated CNTs.

2.2. Characterization methods

X-ray diffraction patterns (XRD) of the samples were recorded on a Rigaku diffractometer using Cu Kα irradiation. TEM and

Cite this: DOI: 10.1039/c0xx00000x

www.rsc.org/xxxxxx

ARTICLE TYPE

HRTEM measurements were conducted on a FEI-Tecnai 12 electron microscope operated at 100 Kv and a JEOL JEM 2010 electron microscope operated at 200 Kv, respectively. A Shimadzu spectrophotometer (model 2501 PC) equipped with an integrating sphere was used to record the UV-vis diffuse reflectance spectra of the samples. Thermogravimetric analyses (TGA) were carried out on a Shimadzu DTG-60/60H thermal analyzer under a air flowing rate of 50 cm^3 min^{-1} and a heating rate of 10 °C min^{-1}. The photoluminescence (PL) spectra were checked by using LS 50B (Perkin Elmer, Inc., USA).

2.3 Photocatalytic reaction

Photocatalytic water splitting was carried out in a LabSolar□photocatalytic H_2 evolution system (Perfectlight, Beijing) with a 300 W Xe lamp (PLS-SXE300, Beijing Trusttech) with a UV cut-offfilter (λ≥ 420nm). In a typical process, 50 mg of SiC or SiC-CNTs powder was dispersed in a Pyrex glass reactor containing 100 mL of 0.1 M Na_2S solution. Then the system was sealed and vacuumized to keep the pressure at -0.1 MPa. Afterwards, a circular cooling water system was turned on and the reactor was irradiated with Xe lamp (300 W) under magnetic stirring. The gases evolved were analyzed on line with a gas chromatograph (GC-7900, TCD, with N_2 as carrier gas) after 1 h of illumination. The reaction was continued for 5 h.

3. Results and discussion

3.1. XRD

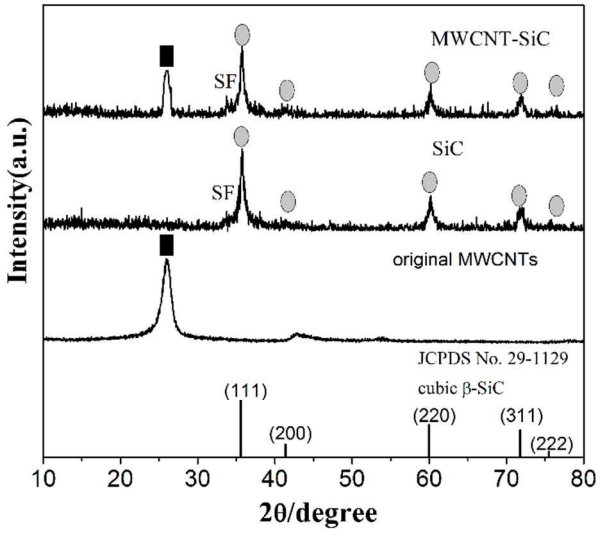

Fig. 1 Powder X-ray diffraction patterns of pure SiC and the SiC-CNTs composite.

The crystal structure of as-synthesized samples was identified by powder XRD method. Fig. 1 shows the powder XRD diffraction patterns of pure SiC and SiC-CNTs nanocomposites. As shown in Fig.1, it is found that the diffraction peaks at 2θ values of 35.66°, 41.42°, 59.99°, 71.76° and 75.51° can be indexed to the (111), (200), (220), (311) and (222) reflections of 3C-SiC phase, respectively,[45, 46] indicating the formation of pure 3C-SiC (JCPDS Card No. 29-1129). The sharp diffraction peaks of samples with strong intensity further indicated the good crystallinity of the as-grown 3C-SiC samples. The appearance of low-intensity peak marked with SF near 2θ = 33.5° is due to the stacking faults within the β-SiC.[47] The calculated lattice constant (a = 4.351 Å) is close to the reported values of β-SiC (a = 4.359 Å, JCPDS card no. 29-1129). The remarkablely enhanced (111) peak suggests the preferential anisotropic growth orientation of the product. Besides the peaks of β-SiC phase, there is an apparent XRD peak at 26.2° in the SiC-CNTs nanocomposites, which is the characteristic peak for MWCNTs.[35, 48] No noticeable diffraction peaks of impurities, such as Si and SiO_2, were detected in this pattern, indicating that the as-prepared SiC-CNTs nanocomposites were composed of β-SiC (or 3C-SiC) and CNTs.

3.2. TEM

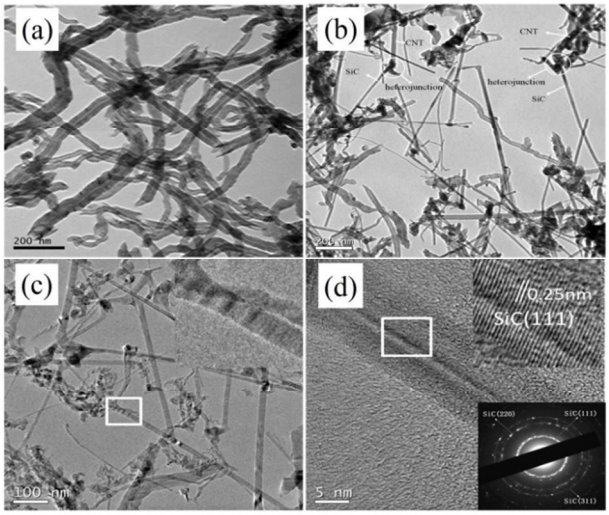

Fig. 2 Transmission electron microscopy (TEM) image of (a) CNTs, (b) SiC-CNTs, (c) SiC and Enlarged TEM (inset, up), (d) HRTEM of SiC and Enlarged HRTEM (inset, up) and the corresponding SAED pattern (inset, bottom).

In order to analyze the morphology and microstructure of the samples, TEM was also performed.TEM images of three samples are shown in Fig. 2. From these images, the CNTs sample consists of nanotubes with diameters from 20 to 40 nm and lengths up to hundreds of micrometers (Fig. 2a). The nanotubes are randomly oriented and have a smooth surface and a crooked morphology. The metal-free SiC-CNTs sample prepared from CNTs consists of crooked nanotubes, straight SiC nanowires and nanoparticles (Fig. 2b). It was also observed from Fig. 2b that SiC nanowires and some nanoparticles (imcomplete growth) were connected to the surfaces of carbon nanotubes. The metal-free MWCNTs/SiC 1D-1D nanoheterostructures are also shown in Fig. 2b. Fig.2c shows the typical TEM image of the nanowires, revealing that the SiC nanowires have smooth surfaces and parallel stacking faults (The inset in Fig. 2c).[24] Typically, the straight SiC nanowires have an average diameter of 10–30 nm and a maximum length of up to microns. Although the diameters

of the as-synthesized SiC nanowires were similar to or much smaller than those of the carbon nanotubes, the SiC nanowires are randomly oriented with straight morphologies. The results showed that the SiC nonowires were not mainly formed by means of the carbon nanotubes-confined reaction.[38, 49, 50] Fig.2d shows the typical HRTEM image of the SiC nanowires. The inset in Figure 2d (up) shows clear lattice fringes for the (111) planes β-SiC with a d-spacing of 0.25 nm, which matches well with the reported value.[51] The selected-area electron diffraction (SAED) pattern (inset in Figure 2d, bottom) can be indexed to β-SiC.

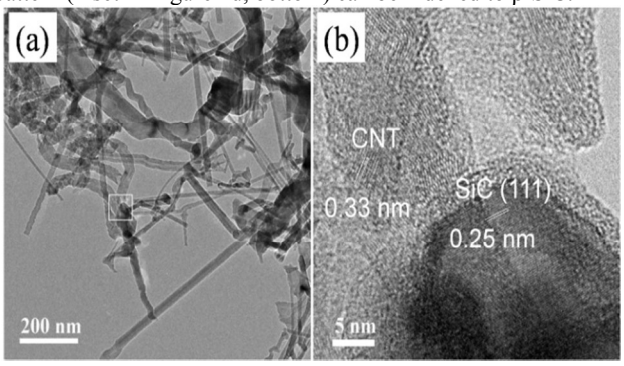

Fig. 3 TEM image of MWCNTs/SiC nanoheterostructures (a), and the corresponding HRTEM image (b).

To further highlight the nanoheterostructures in the MWCNTs/SiC composite. TEM and HRTEM images of MWCNTs/SiC nanoheterostructures were measured and shown in Fig. 3a and 3b, respectively. As shown in Fig. 3b, the HRTEM image of MWCNTs/SiC composite shows two different crystal lattices. The lattice fringes of with spacing of *ca.* 0.25 and 0.33 nm were attributed to the crystal facets of (111) and (002) of 3C-SiC and MWCNTs, respectively.[51-53] Furthermore, a close interface between MWCNTs and SiC could be clearly observed, revealing the formation of the nanoheterostructures. As a result, the efficient hole-electron separation in SiC and electron transfer between the MWCNTs and SiC would be achieved, which is of great importance for the improvement of photocatalytic activity. This also demonstrates that the "*in situ*" growth of SiC nanowires on MWCNTs could create a perfect heterostructure rather than a simple physical mixture between them.

3 Proposed growth mechanism of SiC nanostructures

Control experiments have shown that the SiC nanowires could be formed only in the presence of La and Ni residues. The presence of La and Ni residues were necessary in the reaction to produce the SiC nanowires. As shown in **Fig.S1**, only the SiC nanotubes were obtained in the absence of La and Ni residues after the MWCNTs were washed with a mixed H_2SO_4/HNO_3 solution at 70 ℃ for 12 h.

In our case, through heating the MWCNTs and silicon powder in an argon atmosphere at 1320℃ for 4 h, the formation of SiC nanowires here is mainly involved in a chemical reaction between solid-carbon nanotube and Si powder (see Eq. 1).

$$Si + C \rightarrow SiC \quad (1)$$

In order to shed light on the growth mechanism of the SiC nanowires in the presence of La and Ni residues, we resort to the vapor-liquid-solid (VLS) mechanism shown in Fig. 4A.[54, 55] Since the melting points, T, of pure La and Ni metals are 921 °C and 1453 °C, respectively, La-Ni alloy is expected to form La–Ni liquid droplets (Figure 3A) under 1320 °C. In this VLS mechanism, the liquid La–Ni droplets play a crucial role in acting as catalysts to absorb and dissolve reactant species, e.g., Si (g), and guide the growth of the SiC nanowires along MWCNTs. This process may consist of three important steps: i) production of liquid La–Ni droplets and Si (g) by the sublimation of solid Si powder; ii) chemical reaction (1) at the solid MWCNT-liquid La–Ni droplet interface; and iii) MWCNT loss and growth of the SiC nanowires at the liquid–solid interface.

After the MWCNTs were washed with a mixed H_2SO_4/HNO_3 solution at 70 °C for 12 h, the reaction type between the MWCNTs and silicon powder changes from the VLS reaction to a vapour-solid reaction, and the formation of SiC nanotubes (Fig. 4B) in the absence of La and Ni residues is mainly attributed to the vapour-solid reaction between solid-carbon shells and Si vapour on the outer surface of the MWCNTs (see Eq. 1).

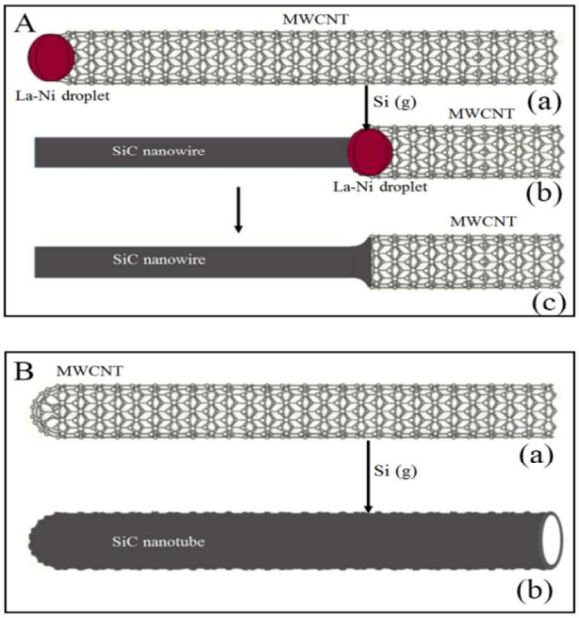

Fig. 4 A) Illustration of the growth process of SiC nanowires. The liquid La-Ni droplet attached on MWCNT (a). MWCNT loss and growth of the SiC nanowires at the liquid–solid interface (b). The obtained SiC/CNTs heterostructure after La-Nicatalysts were removed (c). B) MWCNT (a). SiC nanotube after the vapour-solid reaction of the MWCNTs and Si vapour (b).

3.4. UV-Vis absorption spectra

The optical property of SiC-CNTs nanocomposites was characterized using UV-Vis absorption spectra. Fig. 5 shows the UV-Vis absorption spectra of SiC, R-SiC and SiC-CNTs nanocomposites. Obviously, all the samples exhibit a wide absorption band from UV to visible light and a similar absorption edge of 545 nm. Thus, their corresponding band gaps are estimated to be roughly 2.3 eV on the basis of the UV-Vis absorption spectra. Furthermore, it is also seen from Fig. 5 that the visible-light absorption of SiC-CNTs nanocomposites is stronger than that of pure SiC and R-SiC, indicating that the SiC-CNTs nanocomposites have better visible-light response than pure SiC，which will be beneficial for the improvment of the photocatalytic activity.

Cite this: DOI: 10.1039/c0xx00000x

www.rsc.org/xxxxxx

ARTICLE TYPE

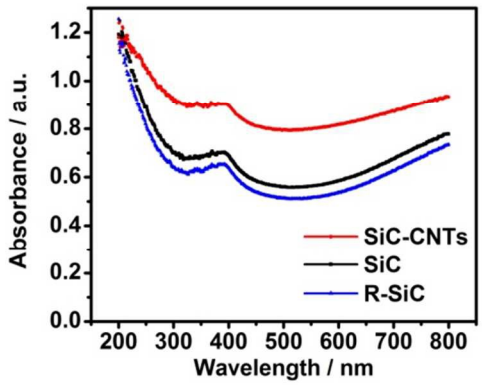

Fig. 5 UV-Vis absorption spectra of SiC,R-SiC and SiC-CNTs nanocomposites

3.5 Thermogravimetric analyses (TGA)

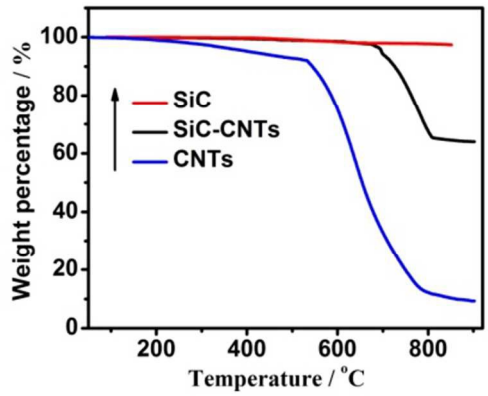

Fig. 6 TGA profiles of SiC-CNTs nanocomposites, pure SiC and CNTs.

The thermal behavior of samples was investigated in order to evaluate the stability of as-synthesized composites. Fig. 6 shows the variation of the TGA profiles of metal-free SiC-CNTs nanocomposites, pure SiC and CNTs during calcination in N_2 up to 800 °C. As depicted in Fig. 6, it is found that pure SiC is quite stable up to 800 °C since there is no significant weight loss (2.5%) was observed at this temperature range. However, the SiC-CNTs nanocomposites are not as stable as pure SiC. For the SiC-CNTs nanocomposites (Fig. 6), there is a substantial weight loss (36%) in the temperature 700–800 °C, corresponding to the content of CNT in the metal-free SiC-CNTs nanocomposites. It is clear that the oxidation temperature is higher than that of pure CNTs (between 550 and 750 °C).[56] The results demonstrate that the introduction of SiC can markedly enhance the thermal stability of CNTs, which has been observed by other researchers.[57] This high resistance towards oxidation was attributed to the formation of CNTs/SiC 1D-1D nanoheterostructures, which can increase the diffusion barrier of oxygen. The TG results further demonstrate the existence of CNTS in the metal-free SiC-CNTs nanocomposites. Moreover, according to the TG curves, the content of CNT in the SiC-CNTs nanocomposites was estimated to be about 36%.

3.6 Photocatalytic H_2-evolution efficiency

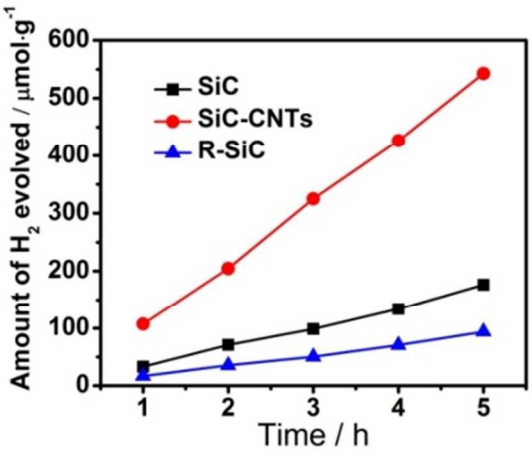

Fig. 7 H_2 evolution over SiC, R-SiC and SiC-CNTs nanocomposites under visible light irradiation. Experimental conditions: 50.0 mg photocatalysts, 100 mL 0.1 M Na_2S solution, 300 W Xe lamp solar simulator with a UV cut-off filter ($\lambda \geq$ 420nm).

Hydrogen evolution over SiC, R-SiC and SiC-CNTs nanocomposites under visible light irradiation is shown in Fig. 7. Control experiments show no appreciable H_2 evolution in the absence of either photocatalyst or light irradiation. This was different from the recent study by Yang et al., in which they found that the obvious H_2 generation from direct chemical reaction between SiC and water in dark could partially contribute to the total photocatalytic activity of SiC.[27] This difference further suggests that no grain surface evolution takes place on the surface of SiC nanowires, since their stability could be efficiently enhanced by the formation of CNTs/SiC 1D-1D nanoheterostructures. As observed in Fig. 7, it is clear that the SiC-CNTs nanocomposites have a much higher photocatalytic activity than the pure SiC and R-SiC. The rates of hydrogen production over the SiC, R-SiC and SiC-CNTs composites are calculated to be 35.2, 18.7 and 108 μmol/g.h, respectively. Average H_2 evolution rate over the SiC-CNTs nanocomposites is 3.1 and 5.8 times higher than those of the unmodified SiC and R-SiC, respectively, due to the introduction of 36 wt% CNTs. Therefore, it is clear that the loaded CNTs play an important role in determining the H_2-evolution rate of metal-free SiC-CNTs nanocomposites. The similar improvements of H_2-evolution rate have been fully confirmed in many other systems such as CNTs/TiO_2,[52] CNTs/$Cd_{1-x}Zn_xS$,[58, 59] CNTs/CdS[60, 61] and CNTs/C_3N_4[62, 63]. In generally, the H_2-evolution rate could be enhanced by a factor of 1.5-4 due to the loading of CNTs onto the

semiconductors. Particularly, a more than 10-fold enhancement in H_2-evolution rate could also be achieved by further optimizing the Schottky-type interfaces between CNTs and semiconductors or loading the third component such as co-catalysts.[60, 64]

To deeply understand the important roles of CNTs in enhancing the H_2 evolution rate of SiC nanostructures. Some previously reported SiC-based photocatalysts for H_2 production were summarized in **Table 1**. As shown in Table 1, there is a significant difference in their activities for H_2 production. Clearly, the H_2-evolution rate of SiC-CNTs nanocomposites in this work is much larger than those of commercial SiC and other SiC prepared using other carbon sources. Furthermore, it is also observed that the H_2-evolution rate over SiC-CNTs nanocomposites is also larger than those reported for the SiC-graphene composites.[10, 31] However, the highest activity in this work is also more than an order of magnitude less than those of simple ternary and quaternary composites,[11, 21] implying that the H_2-generation activity of SiC-CNTs nanocomposites in this work could be further enhanced through multiple hybrids or loading suitable co-catalyst in future studies. In particular, the ternary hybridization of SiC, CNTs and suitable co-catalysts such as MoS_2 may represent one promising direction to construct highly efficient SiC-based composite photocatalysts for solar hydrogen generation from water splitting.[29, 65]

Table 1 Comparison of β-SiC-36 wt% CNTs sample with other SiC-based photocatalysts for their H_2-production activities

Photocatalyst	Synthesis conditions	Modifier	Light source	mass (g)/solution	Activity (μmol g^{-1} h^{-1})	Enhanced factor	Ref.(year)
β-SiC	Carbothermal reduction/ Argas,1320 °C,6 h ,0.1 MPa	36wt% CNTs	300 W Xe, λ ≥ 420 nm	0.05/ 100ml0.1 M Na_2S	108	3.1	This work
Ultrafine β-SiC powder	arc-plasma furnace/0.1 MPa,Ar/H_2(50 vol %)		400 W Xe,260 to 410 nm	0.01/ pure water	91		[32](1990)
Commerciala-SiC (hexagonal)			150 W Xe, 1mM$NaNO_2$	0.05/40mlH_2O, pH 12	53.6		[33](2007)
Commercial β-SiC nanoparticles			150 W Xe, AM 1.5	0.02/ 100.0mL deionized water	36		[28](2014)
3C–SiC			300 W Xe, λ ≥ 420 nm	0.1/ 100 mL 0.3 M KI	11		[27](2013)
worm-likeβ-SiC nanowires	Carbothermal reduction/ Argas,1300 °C,6 h,0.1 MPa		300 W Xe, λ≥420 nm	0.1/ 100 mL distilled water	3.75		[26]2013)
Acid oxidation β-SiC nanowires	Carbothermal reduction/ Argas,1300 °C,6 h,0.1 MPa		350 W Xe, λ≥420 nm	0.1/ 100 mL distilled water	3.62	1.76	[24]2012)
β-SiC	chemical grafting method	3.7 wt% /RGO	300 W Xe, Λ>420 nm	0.1/ 100 mL distilled water	3.91	1.92	[10](2013)
3C-SiC nanopowder	wet chemistry method	1wt% /RGO	300 W Xe,λ ≥ 420 nm, 160mW.cm^{-2}	0.1/ 100 mL 0.3 M KI	~42.41	1.3	[31](2013)
SiC	wet chemistry method	50 wt%CdS	300 W Xe, λ≥420nm	0.05/ 100 mL 0.1 M Na_2S and 0.1 M Na_2SO_3	555		[11](2014)
SiC/CdS composite (mass ratio 1 : 0.5)	wet chemistry method	3 wt% Pt	300 W Xe, λ≥420 nm	0.05/ 100 mL 0.1 M Na_2S and 0.1 M Na_2SO_3	5460	10	[11](2014)
3C-SiCnanowires	Sol-gel carbothermal reduction,1500 °C,5 h	5 wt% Pt	300 W Xe lamp	0.02/ 100 mL distilled water	204	1.88	[29](2014)
SiC/TiO_2 (mass ratio 1 : 1)	sol–gel and impregnation methods	0.75 wt% Cr_2O_3	500 W Xe, λ≥400 nm	0.2/50 mL(Na_2S:Na_2SO_3 =5:1, in mass)	28.2	4	[66](2012
SiC	vapour–solid reaction/Argas,1320 °C,4 h	7.1 wt% SnO_2	300 W Xe, White light	0.35 M Na_2S and 0.25 M Na_2SO_3	825	1.65	[23](2014)
IrO_2/SiC(1wt%)-NiO_x/TiO_2	Ultrasonic impregnation methods		300 W Xe	0.03/60 mL 16 v% ethanol	5826		[21]2013)

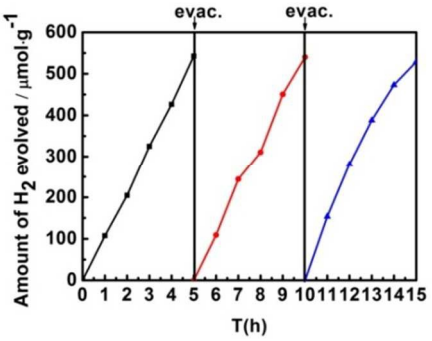

Fig. 8 Repeated runs of photocatalytic H_2 evolution using the SiC-CNTs heterostructures.

Apart from the photocatalytic activity, the photostability of a given photocatalyst is also crucial for its practical applications in sustainable reuse.[1] The stability of the SiC-CNTs heterostructures as H_2-production photocatalysts was further evaluated by recycling the photocatalyst under visible light irradiation for 15 h. Fig. 8 shows the repeated runs of photocatalytic H_2 evolution using the SiC-CNTs heterostructures. As observed in Fig. 8, there is no apparent loss in the photoactivity for the SiC-CNTs nanocomposites after the 3-cycle test, further demonstrating that the SiC-CNTs heterostructured photocatalysts also exhibit excellent stability during photocatalytic H_2 production.

3.7 Proposed photocatalytic enhancement mechanism

To further investigate the mechanism of photocatalytic reaction over SiC-CNTs nanocomposites, the photoluminescence (PL) spectra of SiC, R-SiC and SiC-CNTs photocatalysts was performed, which is useful for investigating the migration, transfer, and recombination processes of the photogenerated electron-hole pairs in the semiconductor.[67] Fig. 9 gives the PL spectra of SiC, R-SiC and SiC-CNTs photocatalysts at an excitation wavelength of 220 nm. As shown in Fig. 9, the emission wavelength ranging from 440 to 560 nm should be attributed to the quantum confinement of 3C-SiC

nanocrystallites.[18] It is clear that the R-SiC exhibited the stronger intensity than pure SiC and SiC-CNTs nanocomposites. This results match well with the above photo-activity measurements and discussions, which further indicated that the CNTs in the compositecan effectively suppress the recombination of photogenerated holes and elcrtrons. Thus, the separation of photo-generated charge carriers is crucial to the photocatalytic activity enhancements.

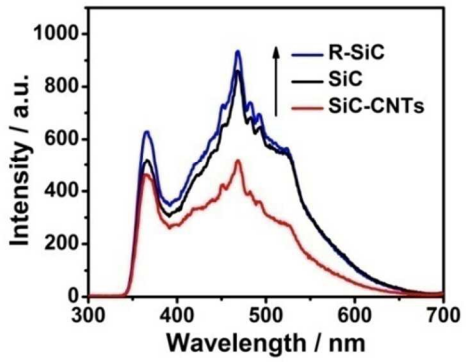

Fig. 9 PL spectra of SiC, R-SiC and SiC-CNTs photocatalysts at an excitation wavelength of 220 nm

The schematic illustration of the charge transfer behavior at the interface between SiC and CNTs and a possible atomic-scale H_2-production mechanism over SiC-CNTs composite photocatalysts were also proposed and shown in Fig. 10. Recently, it has been experimentally and theoretically verified that the dissociation of water and pre-existing hydrogenated surface Si−H sites are crucial for the high H_2-evolution activity of SiC nanocrystals.[68, 69] Four main chemical reactions were shown in Eq. 2-5.

$$Si\text{-}H + H_3O^+ \rightarrow Si\text{-}H\cdot\cdot\cdot H_3O^+ \quad (2)$$

$$Si\text{-}H\cdot\cdot\cdot H_3O^+ + e^- \rightarrow Si + H_2 + H_2O \quad (3)$$

$$Si + e^- \rightarrow Si^- \quad (4)$$

$$Si^- + H_3O^+ \rightarrow Si\text{-}H + H_2O \quad (5)$$

There are two main reasons for the enhancement of the photocatalytic activity after the formation of the Schottky-type junction between SiC and CNTs in the SiC-CNTs nanocomposites. On the one hand, it is well known that CNTs have a large electron-storage capacity (one electron per 32 carbon atoms)[70] and lower work function (4.3 eV for MWCNTs).[71] Once the Schottky-type junction between SiC and CNTs in the SiC-CNTs nanocomposites was formed, the photon-excited electrons from excited SiC nanowires can migrate into the conducting network of MWCNTs, thus suppressing the recombination of photo-excited electron-hole pairs and accelerating the reactions (3) and (4) on the surface of SiC nanowires. As a result, an enhanced H_2-evolution activity was achieved. On the other hand, CNTs can provide more active sits for the photocatlytic hydrogen evolution reaction, which are also beneficial for the enhancement in photocatalytic activity of SiC. Furthermore, the stored electrons in the CNTs can also be directly transferred to the adjacent surface H_2-evolution sites ($Si\text{-}H\cdot\cdot\cdot H_3O^+$), and thus significantly promoting the reactions (3) and (4) on the surface of SiC nanowires. In a word, CNTs in the SiC-CNTs nanoheterostructures play important roles in improving photocatalytic activity of SiC, which can not only increase the surface active sites, but also greatly promote the charge separation and accelerate the reactions (3) and (4) on the surface of SiC nanowires. Therefore, a significant enhancement of the photocatalytic H_2-evolution activity was achieved due to the formation of SiC-CNTs nanoheterostructures.

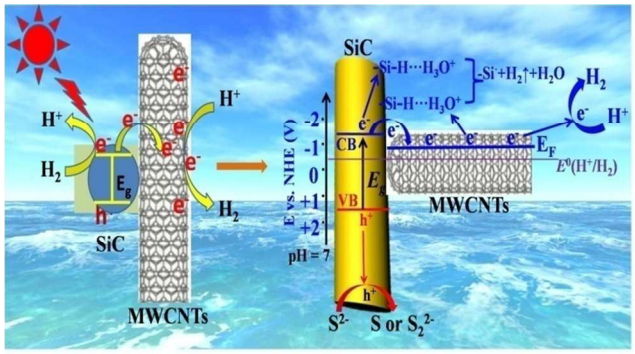

Fig. 10 Schematic illustrations of charge transfer behavior at the interfaces between SiC and CNTs and a possible photocatalytic H_2-production mechanism over SiC-CNTs composite photocatalysts.

4. Conclusions

In conclusion, the SiC-CNTs heterostructures were synthesized by an *in situ* chemical reaction between MWCNTs and silicon powders. The metal-free SiC-CNTs 1D-1D heterostructures exhibited better visible light absorption capacity and thermal stability. Average rates of hydrogen production over the metal-free SiC-CNTs 1D-1D heterostructures can reach up to 108 μmol/g.h, which is 3.1 times higher than that of the unmodified SiC. The improved photocatalytic activity can be attributed to the enhanced the separation of photo-generated holes and electrons and the increased visible light absorption. Thus, our results demonstrate a highly effective strategy for developing SiC-CNTs and other carbon-containing composite photocatalysts for photo-induced hydrogen production from water splitting under visible light irradiation.

5. Acknowledgements

The work was supported by the National Natural Science Foundation of China (20906034, 20963002, 21173088, 21207041 and 21475047). Special thanks to Prof. Can Li in State Key Laboratory of Catalysis, Dalian Institute of Chemical Physics, Chinese Academy of Sciences. This work also partly supported by the State Key Laboratory of Catalysis cooperation project (N-08-08) and the State Key Laboratory of Advanced Technology for Material Synthesis and Processing (2015-KF-7).

Notes and references

School of Materials and Energy, South China Agricultural University, Guangzhou 510642, China. E-mail: Xinliscau@yahoo.com (X. Li), ypfang@scau.edu.cn (Y. Fang)

†Electronic Supplementary Information (ESI) available: [details of any supplementary information available should be included here]. See DOI: 10.1039/b000000x/

‡ Footnotes should appear here. These might include comments relevant to but not central to the matter under discussion, limited experimental and spectral data, and crystallographic data.

1. X. Li, J. Yu, J. Low, Y. Fang, J. Xiao and X. Chen, *J. Mater. Chem. A*, 2015, **3**, 2485-2534.
2. X. Chen, S. Shen, L. Guo and S. S. Mao, *Chem. Rev.*, 2010,

110, 6503-6570.
3. M. Hoffmann, S. Martin, W. Choi and D. Bahnemann, *Chem. Rev.*, 1995, **95**, 69-96.
4. A. Fujishima and K. Honda, *Nature*, 1972, **238**, 37-38.
5. T. Hisatomi, J. Kubota and K. Domen, *Chem. Soc. Rev.*, 2014, **43**, 7520-7535.
6. X. Chen, L. Liu, P. Y. Yu and S. S. Mao, *Science*, 2011, **331**, 746-750.
7. R. Asahi, T. Morikawa, T. Ohwaki, K. Aoki and Y. Taga, *Science*, 2001, **293**, 269-271.
8. X. Wang, K. Maeda, A. Thomas, K. Takanabe, G. Xin, J. Carlsson, K. Domen and M. Antonietti, *Nat. Mater.*, 2009, **8**, 76-80.
9. Y. Wang, J. Hong, W. Zhang and R. Xu, *Catal. Sci. Technol.*, 2013, **3**, 1703-1711.
10. Y. W. Wang, X. N. Guo, L. L. Dong, G. Q. Jin, Y. Y. Wang and X. Y. Guo, *Int. J. Hydrogen. Energ.*, 2013, **38**, 12733-12738.
11. Y. Peng, Z. Guo, J. Yang, D. Wang and W. Yuan, *J. Mater. Chem. A*, 2014, **2**, 6296.
12. K. Zhang and L. J. Guo, *Catal. Sci. Technol.*, 2013, **3**, 1672-1690.
13. Y. Wang, J. Wu, J. Zheng, R. Jiang and R. Xu, *Catal. Sci. Technol.*, 2012, **2**, 581-588.
14. J. Yuan, J. Wen, Q. Gao, S. Chen, J. Li, X. Li and Y. Fang, *Dalton Trans.*, 2015, **44**, 1680-1689.
15. S. S. K. Ma, K. Maeda and K. Domen, *Catal. Sci. Technol.*, 2012, **2**, 818-823.
16. K. Maeda, K. Teramura, D. Lu, T. Takata, N. Saito, Y. Inoue and K. Domen, *Nature*, 2006, **440**, 295-295.
17. C. Yuan, A. Steckl, J. Chaudhuri, R. Thokala and M. Loboda, *J. Appl. Phys.*, 1995, **78**, 1271-1273.
18. X. L. Wu, J. Y. Fan, T. Qiu, X. Yang, G. G. Siu and P. K. Chu, *Phys. Rev. Lett.*, 2005, **94**, 026102.
19. J. Y. Fan, X. L. Wu and P. K. Chu, *Prog. Mater. Sci.*, 2006, **51**, 983-1031.
20. J. Akikusa and S. U. M. Khan, *Int. J. Hydrogen. Energ.*, 2002, **27**, 863-870.
21. Y. Li, Z. Yu, J. Meng and Y. Li, *Int. J. Hydrogen. Energ.*, 2013, **38**, 3898-3904.
22. J. Zhang, L. Z. Liu, L. Yang, Z. X. Gan, X. L. Wu and P. K. Chu, *Appl. Phys. Lett.*, 2014, **104**, 231902.
23. X. Zhou, Y. Liu, X. Li, Q. Gao, X. Liu and Y. Fang, *Chem. Commun.*, 2014, **50**, 1070-1073.
24. J. Y. Hao, Y. Y. Wang, X. L. Tong, G. Q. Jin and X. Y. Guo, *Int. J. Hydrogen. Energ.*, 2012, **37**, 15038-15044.
25. H. L. Liu, G. W. She, L. X. Mu and W. S. Shi, *Mater. Res. Bull.*, 2012, **47**, 917-920.
26. J. Y. Hao, Y. Y. Wang, X. L. Tong, G. Q. Jin and X. Y. Guo, *Catal. Today*, 2013, **212**, 220-224.
27. J. J. Yang, Y. R. Yang, X. P. Zeng and W. X. Yuan, *Sci. Adv. Mater.*, 2013, **5**, 155-159.
28. Y. Zhang, T. Xia, P. Wallenmeyer, C. X. Harris, A. A. Peterson, G. A. Corsiglia, J. Murowchick and X. Chen, *Energy Technology*, 2014, **2**, 183-187.
29. M. Wang, J. Chen, X. Liao, Z. Liu, J. Zhang, L. Gao and Y. Li, *Int. J. Hydrogen. Energ.*, 2014, **39**, 14581-14587.
30. J. Tae Song, H. Mashiko, M. Kamiya, Y. Nakamine, A. Ohtomo, T. Iwasaki and M. Hatano, *Appl. Phys. Lett.*, 2013, **103**, 213901.
31. J. J. Yang, X. P. Zeng, L. J. Chen and W. X. Yuan, *Appl. Phys. Lett.*, 2013, **102**, 4.
32. Y. Nariki, Y. Inoue and K. Tanaka, *J. Mater. Sci.*, 1990, **25**, 3101-3104.
33. Y. T. Gao, Y. Q. Wang and Y. X. Wang, *React. Kinet. Catal. Lett.*, 2007, **91**, 12-19.
34. T. Lv, L. Pan, X. Liu and Z. Sun, *Catal. Sci. Technol.*, 2012, **2**, 2297-2301.
35. A. H. Ye, W. Q. Fan, Q. H. Zhang, W. P. Deng and Y. Wang, *Catal. Sci. Technol.*, 2012, **2**, 969-978.
36. M. Zarezade, S. Ghasemi and M. R. Gholami, *Catal. Sci. Technol.*, 2011, **1**, 279-284.
37. K. Woan, G. Pyrgiotakis and W. Sigmund, *Adv. Mater.*, 2009, **21**, 2233-2239.
38. H. Dai, E. W. Wong, Y. Z. Lu, S. Fan and C. M. Lieber, *Nature*, 1995, **375**, 769-772.
39. X.-H. Sun, C.-P. Li, W.-K. Wong, N.-B. Wong, C.-S. Lee, S.-T. Lee and B.-K. Teo, *J. Am. Chem. Soc.*, 2002, **124**, 14464-14471.
40. T. Taguchi, N. Igawa, H. Yamamoto and S. Jitsukawa, *J. Am. Ceram. Soc.*, 2005, **88**, 459-461.
41. B. Weng, S. Liu, N. Zhang, Z.-R. Tang and Y.-J. Xu, *J. Catal.*, 2014, **309**, 146-155.
42. X. Wang, Z. Li, J. Shi and Y. Yu, *Chem. Rev.*, 2014, **114**, 9346-9384.
43. Y. N. Xia, P. D. Yang, Y. G. Sun, Y. Y. Wu, B. Mayers, B. Gates, Y. D. Yin, F. Kim and Y. Q. Yan, *Adv. Mater.*, 2003, **15**, 353-389.
44. R. S. Devan, R. A. Patil, J. H. Lin and Y. R. Ma, *Adv. Funct. Mater.*, 2012, **22**, 3326-3370.
45. G. Xi, S. Yu, R. Zhang, M. Zhang, D. Ma and Y. Qian, *J. Phys. Chem. B*, 2005, **109**, 13200-13204.
46. H. Li, Y. Lei, Y. Huang, Y. Fang, Y. Xu, L. Zhu and X. Li, *J. Nat. Gas. Chem.*, 2011, **20**, 145-150.
47. A. L. Linsebigler, G. Lu and J. T. Yates, *Chem. Rev.*, 1995, **95**, 735-758.
48. Y. Xu, H. Xu, L. Wang, J. Yan, H. Li, Y. Song, L. Huang and G. Cai, *Dalton Trans.*, 2013, **42**, 7604-7613.
49. C. C. Tang, S. S. Fan, H. Y. Dang, J. H. Zhao, C. Zhang, P. Li and Q. Gu, *J. Cryst. Growth.*, 2000, **210**, 595-599.
50. W. Han, S. Fan, Q. Li, W. Liang, B. Gu and D. Yu, *Chem. Phys. Lett.*, 1997, **265**, 374-378.
51. R. Wu, K. Zhou, J. Wei, Y. Huang, F. Su, J. Chen and L. Wang, *J. Phys. Chem. C*, 2012, **116**, 12940-12945.
52. J. G. Yu, T. T. Ma and S. W. Liu, *Phys. Chem. Chem. Phys.*, 2011, **13**, 3491-3501.
53. M. M. Gui, S.-P. Chai, B.-Q. Xu and A. R. Mohamed, *Sol. Energ. Mat. Sol. C.*, 2014, **122**, 183-189.
54. A. M. Morales and C. M. Lieber, *Science*, 1998, **279**, 208-211.
55. J. Hu, M. Ouyang, P. Yang and C. M. Lieber, *Nature*, 1999, **399**, 48-51.
56. Z. Li, B. Gao, G. Z. Chen, R. Mokaya, S. Sotiropoulos and G. L. Puma, *Appl. Catal. B-Environ.*, 2011, **110**, 50-57.
57. Z. G. Cambaz, G. Yushin, S. Osswald, V. Mochalin and Y. Gogotsi, *carbon*, 2008, **46**, 841-849.
58. J. G. Yu, B. Yang and B. Cheng, *Nanoscale*, 2012, **4**, 2670-2677.
59. X. Liu, P. Zeng, T. Peng, X. Zhang and K. Deng, *Int. J. Hydrogen. Energ.*, 2012, **37**, 1375-1384.
60. Y. K. Kim and H. Park, *Energy Environ. Sci.*, 2011, **4**, 685-694.
61. T. Y. Peng, P. Zeng, D. N. Ke, X. J. Liu and X. H. Zhang, *Energ. Fuel.*, 2011, **25**, 2203-2210.
62. L. Ge and C. Han, *Appl. Catal. B-Environ.*, 2012, **117–118**, 268-274.
63. A. Suryawanshi, P. Dhanasekaran, D. Mhamane, S. Kelkar, S. Patil, N. Gupta and S. Ogale, *Int. J. Hydrogen. Energ.*, 2012, **37**, 9584-9589.
64. A. S. Cherevan, P. Gebhardt, C. J. Shearer, M. Matsukawa, K. Domen and D. Eder, *Energy Environ. Sci.*, 2014, **7**, 791-796.
65. X. Guo, X. Tong, Y. Wang, C. Chen, G. Jin and X.-Y. Guo, *J. Mater. Chem. A*, 2013, **1**, 4657-4661.
66. Y. J. Zhang, Y. Xu, T. Li and Y. C. Wang, *Particuology.*, 2012, **10**, 46-50.
67. C. Han, L. Ge, C. Chen, Y. Li, X. Xiao, Y. Zhang and L. Guo, *Appl. Catal. B-Environ.*, 2014, **147**, 546-553.
68. C. He, X. Wu, J. Shen and P. K. Chu, *Nano Lett.*, 2012, **12**, 1545-1548.
69. X. Shen and S. T. Pantelides, *J. Phys. Chem. Lett.*, 2012, **4**, 100-104.
70. A. Kongkanand and P. V. Kamat, *Acs Nano*, 2007, **1**, 13-21.
71. H. Ago, T. Kugler, F. Cacialli, W. R. Salaneck, M. S. P. Shaffer, A. H. Windle and R. H. Friend, *J. Phys. Chem. B*, 1999, **103**, 8116-8121.

Cite this: DOI: 10.1039/c0xx00000x

www.rsc.org/xxxxxx

ARTICLE TYPE

Graphical Abstract

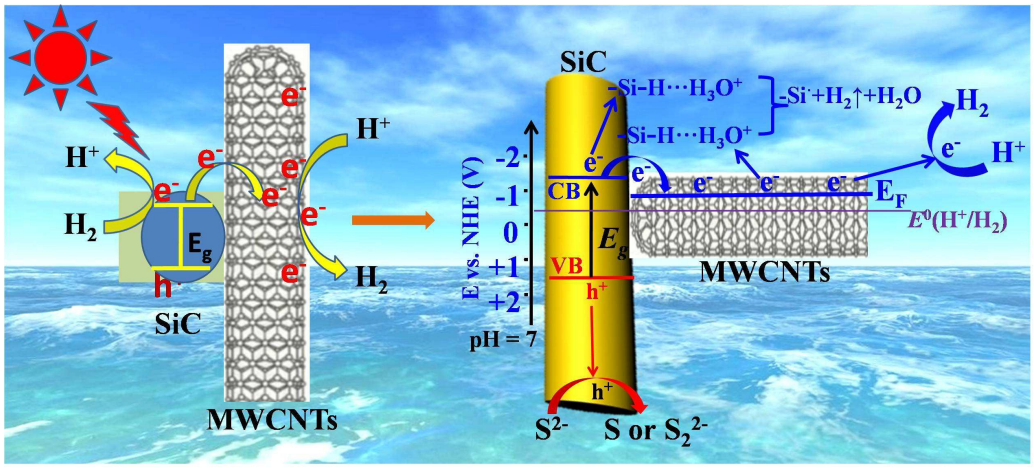

Carbon nanotubes/SiC nanowires 1D-1D heterostructures exhibit significantly enhanced photocatalytic H_2-evolution activities under visible light irradiation.